*Q. J. R. Meteorol. Soc.* (1997), **123**, pp. 1603–1619

# The transient emission of propagating gravity waves by a stably stratified shear layer

By FRANÇOIS LOTT*

*Laboratoire de Météorologie Dynamique du CNRS, France*

(Received 10 April 1996; revised 23 October 1996)

SUMMARY

By analysing the transient evolution of an initial perturbation, it is shown that a stably stratified shear layer emits gravity waves having well defined dynamical characteristics. For instance, the outgoing waves systematically have phase lines tilting against the shear, their vertical momentum flux has a sign opposite to that of the shear and their amplitude increases when the flow stability decreases. Those features are commonly observed in numerical simulations of gravity waves generated by convection. It is shown that they are related to the singular vectors of the system that have fast energy growth and fast energy decay within a finite time. In this work, the singular vectors are computed using a linear gravity-wave model, its adjoint and an iterative Lanczos algorithm. For a given shear layer, characterized by a minimum Richardson number $Ri$ and a depth $d$, these perturbations show that emission of gravity waves by a stratified shear layer essentially occurs for waves with horizontal wave number close to a critical value $k_c = \sqrt{Ri}/d$. The importance of the singular vectors on the dynamics of more general initial conditions is also tested by making few ensembles of numerical simulations with stochastic initial conditions imposed inside the shear layer. The amplitude of the momentum fluxes of the outgoing waves as a function of $Ri$ is also evaluated systematically. It gives a relationship between the efficiency of gravity-wave emission and $Ri$ that could be used in convective gravity-wave parametrization schemes.

KEYWORDS: Gravity waves Shear layer Singular vectors Stochastic initial conditions

## 1. INTRODUCTION

Sources of gravity waves in the atmosphere have received much attention because they are known to influence local meteorology as well as the large-scale atmospheric circulation (Holton 1983; Palmer *et al.* 1986). Important tropospheric sources are believed to include topography (Queney 1947; Smith 1979; Lott and Teitelbaum 1993), convective and frontal activities (Bretherton and Smolarkiewitcz 1989; Shutts and Gray 1994), wind shear (Rosenthal and Lindzen 1983; Fritts 1982; Lott *et al.* 1992) and geostrophic adjustment (Rossby 1937; Blumen 1972). In the context of convection, an important result supported by the observations and the modelling studies (Clark *et al.* 1986; Fovell *et al.* 1992; Alexander *et al.* 1995; Kershaw 1995) is that the efficiency of wave generation depends strongly on the strength of the shear of the horizontal wind. In the presence of shear, waves which are generated have phase lines which tilt upstream (in the frame of reference moving with convection) with height. For these waves, two important questions remain open. What is the fundamental dynamical effect of the shear? Does a selection criterion exist for the horizontal wave number of the waves? One motivation of the present study is to find whether these questions can be answered in a simpler context than convection, when a perturbation is imposed in the shear layer at the initial time and evolves freely thereafter. If some well defined perturbations naturally radiate from the shear layer, it is likely that in the presence of forcing inside the shear, similar structures will be generated.

Without forcing, spontaneous wave generation can occur in a stratified flow as a result of instability when the mean Richardson number is below 0.25 somewhere in the flow (Miles 1961; Howard 1961). In most cases, and when the fluid is unbounded vertically, the instabilities are essentially trapped in the shear layer (see for instance Drazin (1958) and Smyth and Peltier (1989)), but for some mean-flow profiles resonant over-reflection and spontaneous wave generation can occur (Lott *et al.* 1992; Sutherland *et al.* 1994).

* Corresponding address: Laboratoire de Météorologie Dynamique du CNRS, École Normale Supérieure, 24 rue Lhomond, 75231 Paris Cedex 05, France.

In any case, the limitation of these wave-generation processes to flows with minimum Richardson number value smaller than 0.25 is a strong constraint, the Richardson number in the atmosphere being generally larger. This predicts that, in the long term, the free disturbances decay (Booker and Bretherton 1967). Nevertheless, it has long been known that in the stable unstratified Couette flow, inviscid plane waves with phase lines tilting in the direction opposite to the shear experience a temporary amplification before dying away (Orr 1907). Recently these ideas have been actively revived in the literature, in re-examination of barotropic and baroclinic planetary flows (Farrell 1982; Boyd 1983) and bounded stratified shear flows (Farrell and Ioannou 1993). Therefore, it seems relevant to consider whether similar initial conditions producing growth can explain some aspects of the generation of gravity waves by a stratified shear layer.

Nevertheless, the usefulness of these particular disturbances is also questionable (Shepherd 1985). Indeed, in many cases, there are only a few perturbations which lead to significant growth within a given time interval. There are at least as many perturbations that decay and a lot of perturbations for which the energy does not change significantly within the same time interval. Accordingly, it is very unlikely that significant growth can occur with arbitrary initial conditions. Nevertheless, these particular disturbances can also be viewed as the dynamical patterns that control the reorganization of randomly chosen initial conditions towards waves with some well defined characteristics. In this context, it is also essential to study how transient growth from these optimal initial conditions persists, so that well defined perturbations have a chance to dominate the others in the long term. In this respect, the disturbances that decay the most rapidly are also important, they indicate which waves are not to be expected.

In section 2 of the paper the disturbances which grow most rapidly in a finite time interval are obtained by calculating the singular vectors of a linear gravity-wave model using its direct form, its adjoint form and an iterative Lanczos algorithm (Lacarra and Talagrand 1988; Buizza *et al.* 1993). The characteristics of the most rapidly decaying disturbances are also discussed briefly. To separate disturbances which can radiate significant outgoing waves from those which remain trapped in the shear layer, the optimal singular vectors are described for different horizontal wave numbers. In section 3, several ensembles of simulations are presented at various horizontal wave numbers. In these simulations the initial conditions are chosen randomly, over a 'quasi-orthogonal' basis which confines the initial perturbation inside the shear layer without favouring any growing or decaying disturbance. It shows that the singular vectors explain some important aspects of the evolution of more general perturbations, chosen randomly inside the shear layer. For instance, the growing and the decaying singular vectors strongly control the sign and the amplitude of the wave-momentum fluxes that radiate away from the shear layer. In the appendices, the details of the direct model and of its adjoint are presented.

## 2. Estimation of the fastest growing perturbations

### (a) *Basic equations and models*

In the present paper, the linear evolution of a two-dimensional initial perturbation in a stratified shear flow with vertical profiles:

$$\tilde{U}(\tilde{z}) = U_0 \tanh(\tilde{z}/d)\,, \quad \tilde{N}^2 = {N_0}^2\,, \tag{1}$$

is considered, where $d$ is the depth of the shear layer and $\tilde{N}$ is the Brunt–Väisälä frequency. In the following, the equations are written in dimensionless form using $d$, $U_0$, $d/U_0$ and

$N_0{}^2 d$ as units of length, speed, time and buoyancy force. Within the Boussinesq approximation the divergenceless perturbation velocity field can be expressed (with the tildes dropped in non-dimensional form) in terms of a stream function, $\psi$:

$$(u, w) = (-\partial_z \psi, \partial_x \psi) , \tag{2}$$

where $\partial_z$ and $\partial_x$ denote $\partial/\partial z$ and $\partial/\partial x$, repectively. Introducing $\rho$, the dimensionless density perturbation, and neglecting the Coriolis force, the linear evolution of a perturbation follows the equations:

$$\partial_t \Delta\psi = -U\partial_x \Delta\psi + U_{zz}\partial_x \psi - Ri\partial_x \rho - a\Delta\psi - a_z \partial_z \psi + \nu\Delta\Delta\psi , \tag{3}$$

$$\partial_t \rho = -U\partial_x \rho + \partial_x \psi - a\rho + \nu\Delta\rho , \tag{4}$$

$$\Delta = \partial_x{}^2 + \partial_z{}^2 ,$$

where $\partial_t$, $U_{zz}$ and $a_z$ denote $\partial/\partial t$, $\partial^2 U/\partial z^2$ and $\partial a/\partial z$, respectively. The boundary conditions, $\psi = 0$, $\rho = 0$ and $\Delta\psi = 0$, are imposed at the bottom ($z = -L/2 = -45$) and at the top ($z = L/2 = 45$) of the model domain. In (3), $Ri = N_0{}^2 d^2/U_0{}^2$ is the minimum Richardson number of the flow and $\nu$ is the inverse of the Reynolds number. The coefficient $a(z)$ is a Rayleigh damping, introduced to absorb the perturbation in the uppermost and lowermost layers of depth 5, in order to avoid wave reflection at the boundaries and to simulate an infinite domain:

$$a(z) = \begin{cases} 0.5\left\{1 + \frac{\pi}{5}\,(|z| - 42.5)\right\} & \text{if } 42.5 < |z| < 45 \\ 0.5\left[1 - \cos\left\{\frac{\pi}{5}\,(40 - |z|)\right\}\right] & \text{if } 40 < |z| < 42.5 . \end{cases}$$

The mean flow is assumed to be uniform in the horizontal direction and hence the disturbance can be expressed as a sum of independent harmonics with horizontal wave number $k$:

$$\psi(x, z, t) = \Re[\hat{\psi}(z, t)e^{ikx}] , \quad \rho(x, z, t) = \Re[\hat{\rho}(z, t)e^{ikx}] , \tag{5}$$

for which (3) and (4) become

$$\partial_t \Delta\hat{\psi} = -ikU\Delta\hat{\psi} + ikU_{zz}\hat{\psi} - ikRi\hat{\rho} - a\Delta\hat{\psi} - a_z\partial_z\hat{\psi} + \nu\Delta\Delta\hat{\psi} , \tag{6}$$

$$\partial_t \hat{\rho} = -ikU\hat{\rho} + ik\hat{\psi} - a\hat{\rho} + \nu\Delta\hat{\rho} , \tag{7}$$

$$\Delta = \partial_z{}^2 - k^2 .$$

To determine the disturbance evolution, (6) and (7) are discretized in the vertical direction, and the vertical derivatives are estimated by centred finite differences. Defining $\mathbf{X}$ to be the state vector of the discretized system,

$$\mathbf{X}^{\mathrm{T}} = (\mathbf{X}^{2M-4} \cdots \mathbf{X}^1) = (\hat{\psi}^{M-1} \cdots \hat{\psi}^2 \hat{\rho}^{M-1} \cdots \hat{\rho}^2) , \tag{8}$$

the vertically discretized form of (6) and (7) can be written

$$\partial_t \mathbf{X} = \mathbf{A}\mathbf{X} , \tag{9}$$

which gives the forward model definition

$$\mathbf{X}(t) = \mathbf{M}(t)\,\mathbf{X}(0). \tag{10}$$

In (9) and (10) **A** and **M** are two complex $(2M-4)\times(2M-4)$ matrices. Writing the scalar product between two state vectors as

$$\langle \mathbf{X};\mathbf{X}'\rangle = \sum_{i=1}^{2M-4} \mathbf{X}^i \mathbf{X}'^{i*}\,, \tag{11}$$

where $\mathbf{X}'^{i*}$ denotes the complex conjugate of $\mathbf{X}'^{i}$, the adjoint of the model $\mathbf{M}^*(t)$, relative to this scalar product satisfies

$$\langle \mathbf{X};\mathbf{M}(t)\mathbf{X}'\rangle = \langle \mathbf{M}^*(t)\mathbf{X};\mathbf{X}'\rangle\,, \tag{12}$$

i.e. it is the complex conjugate transpose of **M**. The direct model and its adjoint are described with further details in the appendices A and B, respectively. In all the simulations presented, the vertical grid spacing is $\mathrm{d}z \approx 0.02$ and the timestep is $\mathrm{d}t = 0.05$. These values were adopted after verification that model convergence was reached.

### (*b*) *Methodology*

The initial conditions that produce a large amplification in a specified time, $t_0$, are found following a procedure proposed by Buizza *et al.* (1993). To identify the mechanisms leading to the growth of perturbations, the inner product associated with the total energy-density norm has been adopted. As in the unstratified case, any increases of the total perturbation energy density are solely related to a downgradient Reynolds stress $\overline{uw}$, since

$$[-\overline{uw}U_z] > 0, \tag{13}$$

where the average operators are: $[f] = \frac{1}{L}\int_{-L/2}^{L/2} f(z)\mathrm{d}z$ and $\overline{f} = \frac{k}{2\pi}\int_0^{\frac{2\pi}{k}} f(x)\mathrm{d}x$. This follows from the energy density equation which is obtained by integrating (3) and (4) multiplied by $-\psi$ and $Ri\rho$, respectively, over the model domain:

$$\begin{aligned}\partial_t e = &-[\overline{uw}U_z] - a[\overline{u^2} + \overline{w^2} + Ri\overline{\rho^2}] \\ &-\nu\left[\overline{\left(\frac{\partial u}{\partial x}\right)^2} + \overline{\left(\frac{\partial u}{\partial z}\right)^2} + \overline{\left(\frac{\partial w}{\partial x}\right)^2} + \overline{\left(\frac{\partial w}{\partial z}\right)^2} + Ri\overline{\left(\frac{\partial \rho}{\partial x}\right)^2} + Ri\overline{\left(\frac{\partial \rho}{\partial z}\right)^2}\right],\end{aligned} \tag{14}$$

where

$$e = \left[\frac{\overline{u^2}}{2} + \frac{\overline{w^2}}{2} + Ri\frac{\overline{\rho^2}}{2}\right]. \tag{15}$$

For a discretized state vector with vertical step $\mathrm{d}z$, the energy-density norm is

$$\begin{aligned}\|\mathbf{X}\|^2 &= \langle \mathbf{E}\mathbf{X};\mathbf{X}\rangle \\ &= \frac{\mathrm{d}z}{4L}\sum_{i=2}^{M-1}\left\{\left(\frac{\hat{\psi}^{i+1}-\hat{\psi}^{i-1}}{2\mathrm{d}z}\right)\left(\frac{\hat{\psi}^{i+1}-\hat{\psi}^{i-1}}{2\mathrm{d}z}\right)^* + k^2\hat{\psi}^i\hat{\psi}^{i*} + Ri\hat{\rho}^i\hat{\rho}^{i*}\right\},\end{aligned} \tag{16}$$

where **E** is a positive definite matrix. Thus, the energy of a perturbation for a given discretization evolves in time following

$$e(t) = \|\mathbf{X}(t)\|^2 = \langle \mathbf{E}\mathbf{M}(t)\mathbf{X}(0);\mathbf{M}(t)\mathbf{X}(0)\rangle = \langle \mathbf{M}^*(t)\mathbf{E}\mathbf{M}(t)\mathbf{X}(0);\mathbf{X}(0)\rangle\,, \tag{17}$$

and we search for the singular vectors which satisfy the generalized eigenvalue problem,

$$\mathbf{M}^*(t_0)\mathbf{E}\mathbf{M}(t_0)\mathbf{X}(0) = \lambda\mathbf{E}\mathbf{X}(0), \tag{18}$$

where $\lambda$ characterizes the energy growth (or decay) of a singular vector at $t_0$: $\| \mathbf{X}(t_0) \|^2 = \lambda \| \mathbf{X}(0) \|^2$. These singular vectors identify an orthogonal basis for the energy norm, and evolve into orthogonal patterns at $t_0$. This essentially results from the fact that the matrices $\mathbf{M}^*\mathbf{E}\mathbf{M}$ and $\mathbf{E}$ are Hermitian and positive definite. Then, after a suitable coordinate transform ($\mathscr{X} = \mathbf{E}^{1/2}\mathbf{X}$; Buizza *et al.* (1993)), the eigenvalue problem (18) can be solved using an iterative Lanczos algorithm (Lacarra and Talagrand 1988).

### (c) *Results*

For a given flow configuration ($Ri = 1$ and $\nu = 0$), Fig. 1 shows the largest amplification factor, $\lambda$, as a function of $t_0$ and $k$. It shows that for $t_0 > 10$ the maximum energy amplification becomes substantial (i.e. of order 10 and more) and the largest growths occur slightly above $k = 1$. For larger wave numbers, the maximum energy amplification slowly decays as $k$ increases. For wave numbers $< 1$, the energy amplification rapidly decays as $k$ tends towards 0. Further experiments on the sensitivity to the parameter $Ri$ have shown that this pronounced decrease of the optimal growth at small $k$, always occurs when $k < k_c = \sqrt{Ri}$. This is related to the ability of the singular vector to give rise to travelling waves in the far field. Indeed, if we consider that the perturbation outside the shear layer is composed of waves whose intrinsic frequencies, $\omega$, have a magnitude close to $t_0^{-1}$, they propagate vertically outside the shear layer if their vertical wave number, $m(\omega)$, is real:

$$m(\omega)^2 = k^2 \left\{ \frac{Ri}{(kU + \omega)^2} - 1 \right\} > 0 . \tag{19}$$

Equation (19) is the gravity-wave dispersion relation outside the shear layer. Since significant growth generally appears for $t_0 >> 1$ (i.e. $\omega << 1$), and since $\| U \| \approx 1$ outside the shear, condition (19) reduces to $k_c^2 - k^2 > 0$ : initial perturbations lead to significant travelling waves when their horizontal wave number is smaller than $k_c$.

Figure 2 shows the shapes of the stream function and density perturbations associated with the optimal singular vector when $t_0 = 10$ and $k = 0.75$. The perturbation is

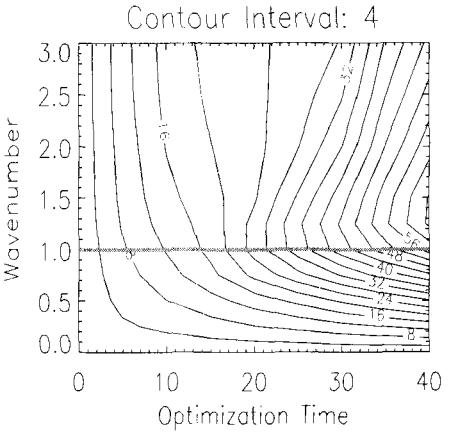


Figure 1. Maximum energy growth as a function of non-dimensional optimization time, $t_0$, and horizontal wave number, $k$. The flow is configured by the minimum Richardson number $Ri = 1$, and the inverse of the Reynolds number $\nu = 0$.

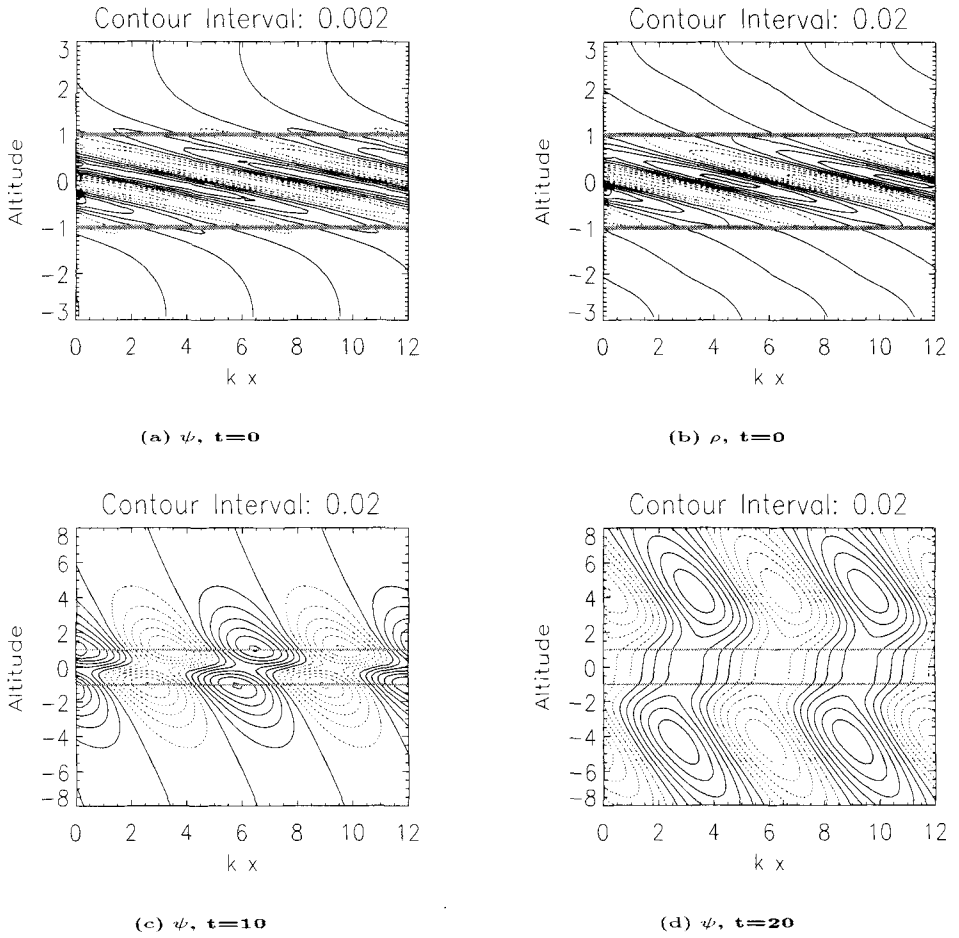


Figure 2. Development of the optimal perturbation in the $x$–$z$ plane. The flow configuration is $Ri = 1$, $v = 0$ as in Fig. 1, with $k = 0.75$ and $t_0 = 10$ (see Fig. 1 for definitions). (a) and (b) show the distributions of the stream function, $\psi$, and the density, $\rho$, at time $t = 0$, and (c) and (d) show $\psi$ at times $t = 10$ and 20, respectively. The grey lines represent the upper and the lower bounds of the shear layer. Note the change in the vertical scale from (a) and (b) to (c) and (d).

initially confined inside the shear layer and has phase lines which tilt against the shear. This indicates an initial downgradient Reynolds stress, as already shown by Farrell and Ioannou (1993). The initial inclination of the phase lines, measured by $-m/k$, is negative and has a magnitude close to $-t_0$. This means that initially the optimal modes have a large vertical wave number, $|m| >> |k|$, whose sign is that of $k$. After $t = t_0$, the optimal perturbation is away from the shear layer and is composed of waves which tilt against the shear, a feature that is often observed for convective waves (Alexander *et al.* 1995; Kershaw 1995). For short, trapped modes, the same fields show that when $t > t_0$ the perturbation remains confined in the shear layer and its phase lines become increasingly inclined in the direction of the shear, indicating an upgradient Reynolds stress and energy decay. This is confirmed in Fig. 3, which shows that the total energy of short, trapped disturbances ($k = 1.25$, $1.5 > k_c = 1$) decays in the long term, while the total energy of the long disturbances ($k = 0.50$, $0.75 < k_c = 1$) is more persistent because they are outside the shear layer when the decay phase starts.

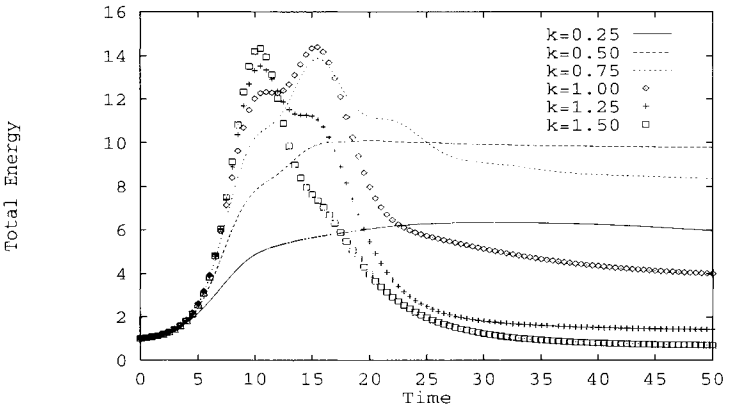


Figure 3. Evolution of the perturbation energy as a function of wave number, $k$. Initial conditions are the optimal initial conditions associated with each different wave number. The flow configuration is $Ri = 1$, $\nu = 0$, and $t_0 = 10$ (see Fig. 1 for explanation).

Vertical sections of the stream-function fields are shown in Fig. 4 at various times and for different horizontal wave numbers. At small wave number, $k = 0.5$, the optimal disturbance develops spectacular gravity waves propagating away from the shear layer. At $t = 40$, the wave field occupies the whole domain, and its amplitude is everywhere larger than that of the initial perturbation. At larger wave numbers, the vertical dispersion of the waves becomes less pronounced, because the vertical velocity of the wave fronts,

$$C_{gz_{\max}} = \max_m \left( \frac{\partial \omega}{\partial m} \right) \approx 0.385 \sqrt{Ri}/k \,,$$

decreases as the horizontal wave number increases. Accordingly, after $t = t_0$ and for $k = 0.75$ and 1.0, the wave fields have well defined travelling fronts where the amplitude is a maximum and beyond which there are no significant perturbations. When $k = 1.25$, the outgoing signal at time $t = 40$ is small and rather close to the shear layer. The wave-front velocity is slow and the signal does not really escape from the shear layer.

A very similar study to the one presented above has also been done for the singular vectors which lead to fast energy decay. Since the basic mechanisms of the decay have been described before for trapped disturbances when $t > t_0$, only a few remarks are given here and further discussion about decaying waves will be given in the next section. As was the case for the fastest growing perturbations, the fastest decaying ones are initially confined inside the shear layer. This means that the influence of the shear in damping initial conditions is also dominant on the time-scales considered in this study. Furthermore, the fastest decaying perturbations are initially slightly inclined in the direction of the shear. This inclination rapidly increases with time producing large upgradient Reynolds stresses that lead to the disturbance decay. In general, the perturbations with $k < k_c$ have a smaller decay than those with $k > k_c$ because they emit a significant number of waves at the beginning of their evolution.

### (*d*) *Influence of diffusion*

Although the growth of outgoing waves is persistent, it is clear that in the inviscid case the largest growths are attained by trapped modes with $k > k_c$. Nevertheless, diffusion can limit this effect because it predominantly dissipates the perturbations with large wave number. Diffusion is also more efficient on the optimal perturbations at large $t_0$ since the

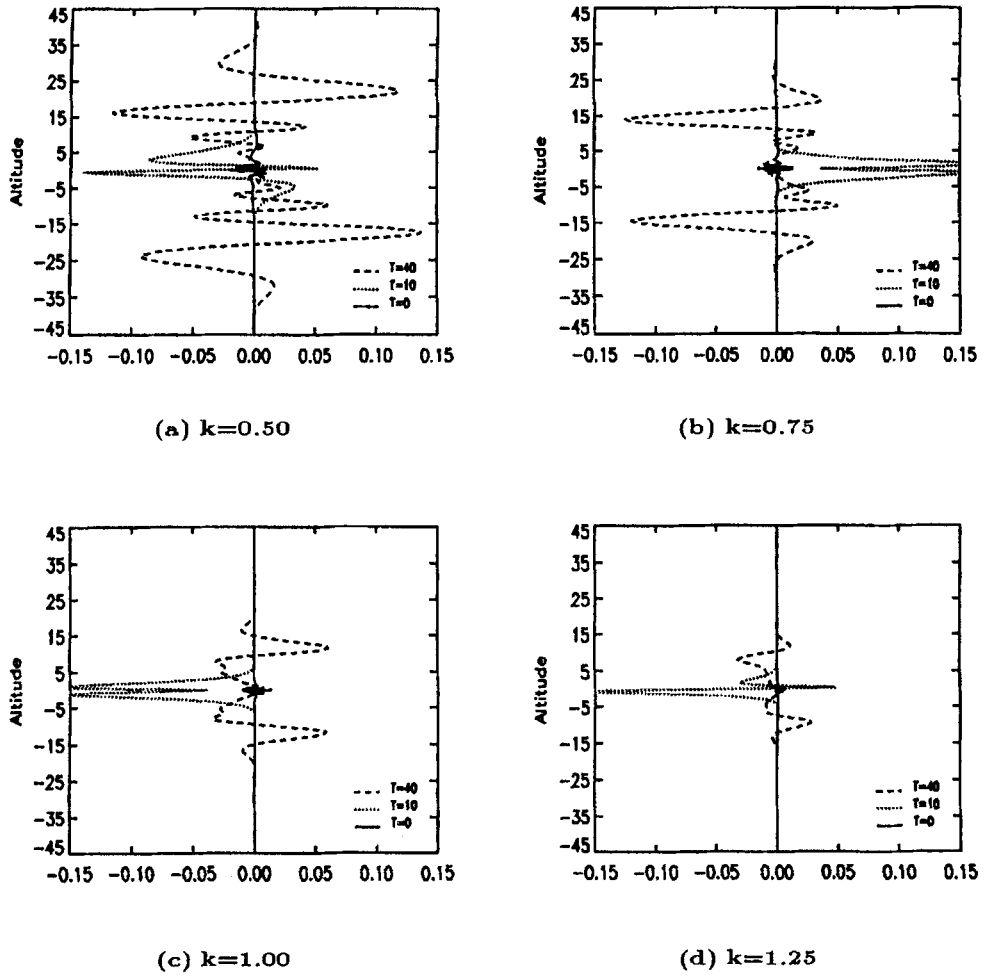


Figure 4. Evolution of the perturbation stream function, from time $t = t_0$ to $t = 40$. The initial conditions in (a)–(d) are the optimal initial conditions associated with four different wave numbers, respectively. $Ri = 1$, $\nu = 0$ and $t_0 = 10$, as in Fig. 3.

vertical wave number of the optimal modes increases with $t_0$. The combination of these two effects means that the maximum energy growth for a given flow configuration (i.e. for given $Ri$ and $\nu$) has a maximum value. For instance, when $Ri = 1$ and $\nu = 10^{-4}$ (Fig. 5) this maximum occurs close to $t_0 \approx 25$ and $k \approx 0.8 < k_c$, in a region where significant outgoing waves can be expected. Further sensitivity experiments on the diffusion parameter, $\nu$, and on the minimum Richardson number, $Ri$, have shown that the largest growth always occurs near $k_c$ (slightly below or slightly above) when $Ri \approx 1$. These sensitivity experiments have also shown that the maximum optimal growth, maximized over $t_0$ and $k$, grows when the flow stability ($Ri$) decreases.

## 3. Stochastic initial conditions

### (a) *General considerations*

The fact that the behaviour of optimal singular vectors may overstate the possible growth of initially small disturbances in a shear flow was noticed by Shepherd (1985). This follows the fact that there are generally only a few initial conditions which give significant

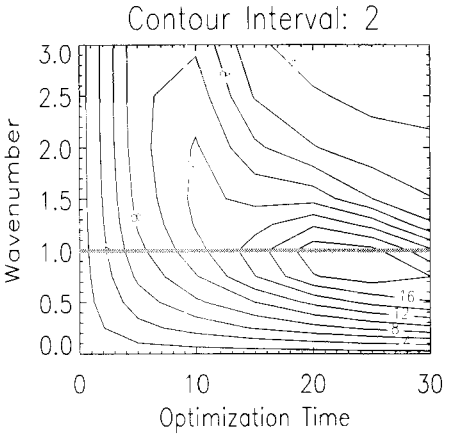


Figure 5. Maximum energy growth as a function of optimization time and wave number, as in Fig. 1, but with flow configuration $Ri = 1$, $\nu = 10^{-4}$.

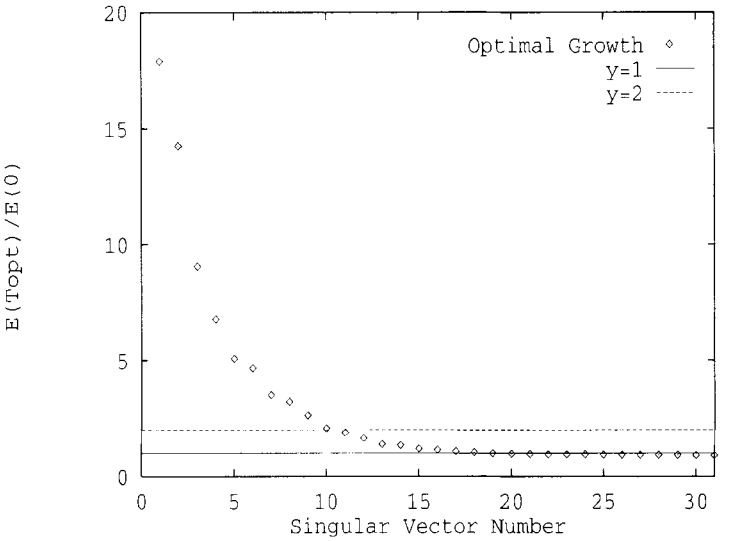


Figure 6. The 30 largest amplification factors for singular vectors optimized over $t_0 = 25$. The amplification factors are stored in decreasing order. $Ri = 1$, $\nu = 10^{-4}$ and $k = 0.75$. See text for explanation.

energy growth within a finite time. Typically, in the flow configuration described here, when $Ri = 1$, $\nu = 10^{-4}$, and close to the optimal configurations $k = 0.8$ and $t_0 = 25$, there are no more than 10 singular vectors which lead to energy amplification exceeding a factor of 2 (Fig. 6). Nevertheless, all this hides the simple fact that the singular vectors indicate how the shear layer filters the perturbation field, favouring certain waves and attenuating others. To illustrate this and to assess whether the physical mechanisms described in section 2 are useful for describing the evolution of more general initial conditions, the behaviour of different disturbances is analysed when the initial conditions are chosen stochastically over a superposition of 'quasi-orthogonal' Gabor functions:

$$\widehat{\psi}_0(z) = \sum_{n=M_0}^{M_1} a_n \phi_n(z) \quad \text{and} \quad \widehat{\rho}_0(z) = \sum_{n=M_0}^{M_1} b_n \phi_n(z) \,, \tag{20}$$

with

$$\phi_n(z) = \exp\left(-\frac{z^2}{2l^2}\right)\exp\left(in\frac{\pi}{2}z\right), \tag{21}$$

and where the amplitudes and the phases of the complex coefficients, $a_n$ and $b_n$, are chosen stochastically between [0, 1] and $[-\pi, \pi]$, respectively. Furthermore, the truncation $M_1 = -M_0 = 12$ is generally adopted. This approximation reduces the number of degrees of freedom to 102 and limits the discussion to perturbations with moderately large vertical wave numbers. The degree of orthogonality of this 'quasi-basis' is measured by

$$\max_{n\neq m}\frac{[\phi_n\phi_m^*]}{[\phi_n\phi_n^*]} = \exp\left\{-\left(\frac{\pi l}{4}\right)^2\right\}. \tag{22}$$

This quantity decreases (i.e. the basis becomes more orthogonal) as $l$ increases. In the following, the value $l = 1.8$ has been chosen and the degree of orthogonality (22) is 0.13. This provides a compromise between the constraint of orthogonality and the desire to confine the initial conditions inside the shear layer.

### (*b*) *Results*

Figure 7 shows the growth of 150 disturbances which are chosen stochastically, with $k = 0.75$, $Ri = 1$, $\nu = 10^{-4}$ and for various truncation parameters $M_0$ and $M_1$. The so-called 'favourable' waves are those for which $M_0 = 1$ and $M_1 = 12$. They have positive vertical wave numbers, with phase lines inclined in the direction opposite to the shear. It is clear that the energy growth, described in section 2 for optimal modes, is found for most of the disturbances chosen in this spectral domain. Even if it is not as large as the optimal growth, some initial conditions in this ensemble reach a growth close to 13. Since the wave number in this ensemble is smaller than $k_c = 1$, the growth is rather persistent, a property that was also indicated by the singular vectors. The so-called 'unfavourable' waves are those for which the vertical wave number is negative, $M_0 = -12$ and $M_1 = -1$. Unsurprisingly, those waves present a rather systematic energy decay. In the last combination, presented in Fig. 7, the truncation is $M_0 = -12$ and $M_1 = 12$, and growth is often observed, even

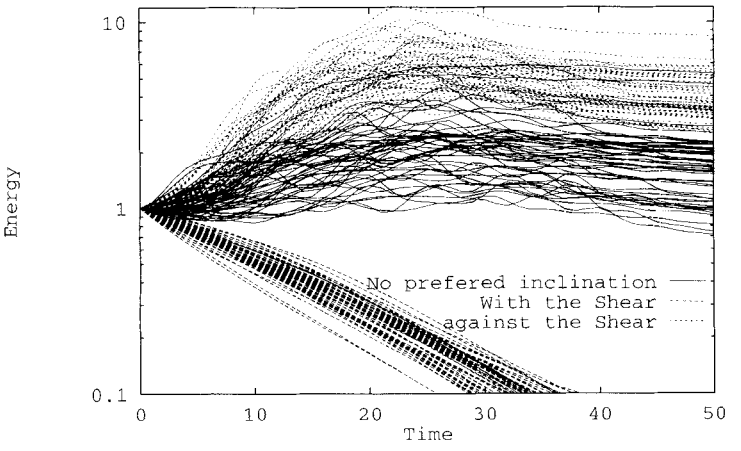


Figure 7. Evolution of the perturbation energy for 150 different initial conditions; 50 'neutral' cases for which $M_1 = -M_0 = 12$, 50 'favourable' cases (against the shear) for which $M_0 = 1$ and $M_1 = 12$ and 50 'unfavourable' cases (with the shear) for which $M_0 = -12$ and $M_1 = -1$ (see text for full definitions and explanation). The flow configuration is $Ri = 1$, $\nu = 10^{-4}$, and $k = 0.75$ (see Fig. 1 for explanation).

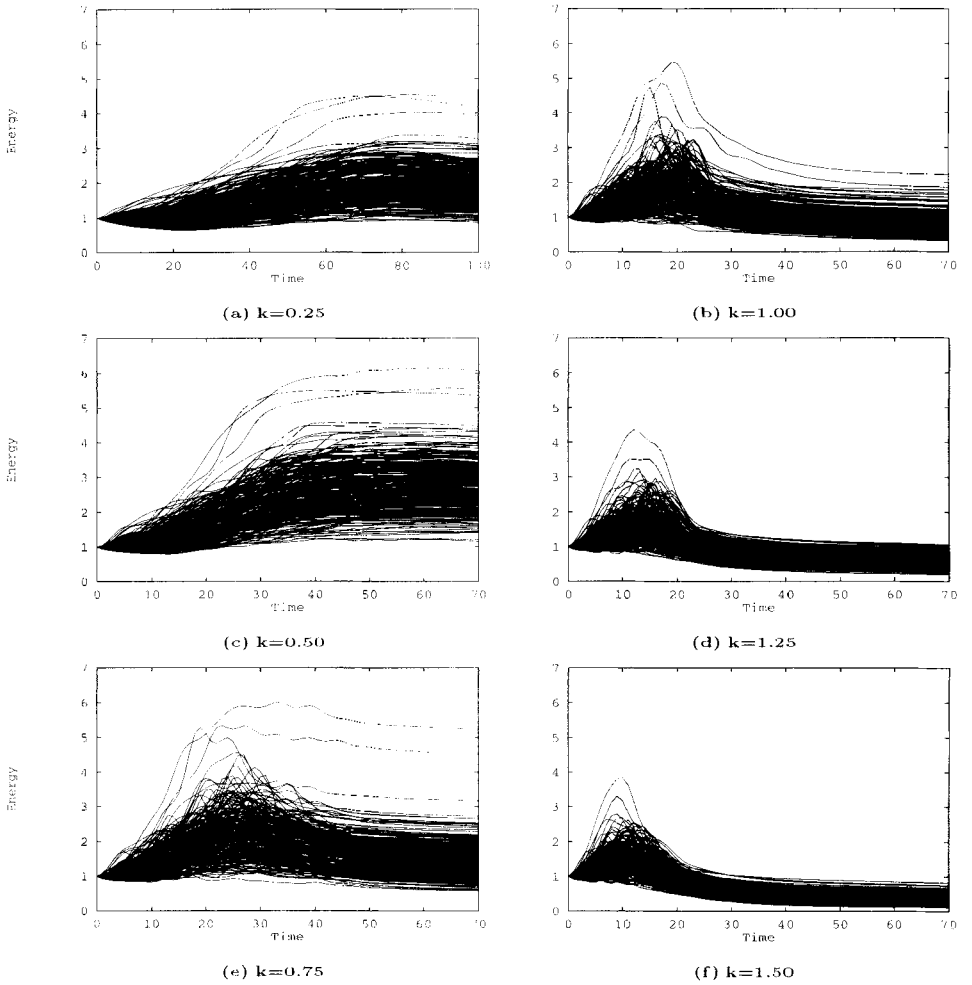


Figure 8. Evolution of the perturbation energy for 200 different initial conditions and for six different values of horizontal wave number, (a)–(f). The flow configuration is $Ri = 1$, $\nu = 10^{-4}$ (see Fig. 1 for definitions).

if it is now limited to 6. The decays associated with the initial conditions which are unfavourable, balance the energy growths associated with the initial conditions which are favourable. Similar experiments, with $M_0 = -12$ and $M_1 = 12$, are shown in Fig. 8 for other horizontal wave numbers. These results illustrate how the energy maintenance found for the optimal singular vectors in section 3 can have important consequences. The long disturbances, with $k = 0.25$ and 0.5, systematically show a larger growth than the short modes with $k = 1.25$, 1.5. It must be noted that the dispersion of the different ensembles of simulations constructed following (21) was very sensitive to the value of the parameter $l$, and to the truncation coefficients $M_0$ and $M_1$. Indeed, the dispersion of an ensemble, with a fixed number of simulations characterized by the variance of the maximum of the energy reached within a realization, decreases when $M_1 = -M_0$ increases beyond 15. At large truncation, more modes with high vertical wave number are introduced, which are essentially attenuated by the diffusion. It was also found that the dispersion decreases when $l$ increases: the less the initial conditions are confined in the shear layer, the less they feel the dynamical impact of the shear.

The preceding experiments have shown that positive shear favours the relatively long disturbances with positive vertical wave number, and damps those with negative vertical wave number. This means that if the disturbance is more or less symmetric initially, the shear will make the waves with positive wave number dominate the far field rather rapidly. Since waves with positive wave number, $m$, have negative momentum fluxes in the far field, as

$$\rho_0 \overline{uw} = \rho_0 \frac{1}{2} \hat{u}\hat{w}^* = -km \frac{\hat{\psi}\hat{\psi}^*}{2}, \tag{23}$$

the shear layer will essentially radiate waves with negative momentum flux. This effect is illustrated in Fig. 9, where a scatter plot of the momentum flux, measured above and below the shear layer and integrated in time until the wave field has completely disappeared, is shown in the case with wind shear and in the case with no wind shear. The initial conditions are those of Fig. 8(b), namely $Ri = 1$, $k = 0.5$, $\nu = 10^{-4}$ and $e(0) = 1$. As mentioned before, with no shear and for initial conditions chosen randomly, the total wave-momentum flux radiating above and below the disturbed area can be either negative or positive and its amplitude never exceeds 0.01. The presence of the positive shear always breaks that symmetry, damping all the waves with negative vertical wave number and amplifying the waves with positive vertical wave numbers. It leads to well defined negative wave-momentum fluxes above and below the shear layer. Furthermore, the filtering by the shear is so efficient that magnitudes of the momentum fluxes are typically 20 times larger than those found without shear. As mentioned in section 2, the optimal disturbance amplification with the shear increases when the flow stability decreases. This effect is also found for the momentum-flux amplification by the shear in the stochastic context. Indeed, the same experiment as that of Fig. 9 has been repeated for many different values of $Ri$ and $k$. It shows that maximum momentum-flux amplification always occurs when $k < k_c$, but is not very sensitive to the value of $k$ provided it is smaller than $k_c$, and is very sensitive to $Ri$. By testing its amplitude for 20 different values of $Ri$ with $0.25 < Ri < 10$, and for different horizontal wave number, it was found that the ratio between the momentum flux with shear and the momentum flux without shear, both averaged over one ensemble of 50

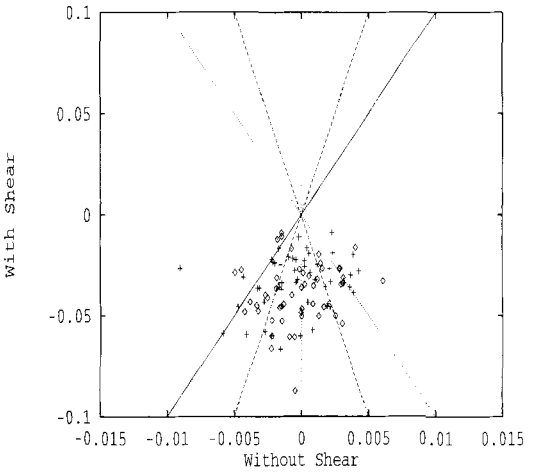


Figure 9. Scatter plot of wave-momentum fluxes with and without shear. The initial conditions are chosen stochastically. Diamonds stand for the momentum flux measured above the layer where the initial conditions are imposed. Crosses stand for momentum flux measured below the layer where the initial conditions are imposed. The flow configuration is $Ri = 1$, $\nu = 10^{-4}$, and $k = 0.75$ (see Fig. 1 for definitions). Lines $y = \pm 10x$ and $y = \pm 20x$ are also shown.

simulations with initial conditions chosen randomly, varies like

$$\frac{8}{Ri} + 20 - Ri \quad \text{when } k < k_c. \tag{24}$$

The ratio exceeds 50 when $Ri = 0.25$ and falls to 10 when $Ri = 10$. Equation (24) is a rather simple fit, which was adjusted empirically, and which is 10% accurate over the 20 different values of $Ri$ which were tested. It is believed that a relationship of this kind should be used as a wave-generation efficiency parameter, close to the parameter $\alpha$ discussed in Kershaw (1995), which links the momentum flux of waves and the convective forcing in parametrization schemes of gravity waves generated by convection. This relationship should nevertheless be used more qualitatively than quantitatively, because it was not tested for other flow configurations nor for many different truncation parameters.

## 4. Conclusions

In this paper, the dispersion of some initial perturbations located in a stably stratified shear flow has been presented. The fastest growing and decaying perturbations over a fixed period of time, $t_0$, were identified using a linear finite-difference wave model, its adjoint and an iterative Lanczos algorithm. They are the singular vectors of the model with the largest and smallest singular values. The simulations show that for all values of the minimum Richardson number and for nearly all wave numbers, there exist perturbations which lead to large energy growth or to large energy decay within a finite time. Initially the growing perturbations are confined inside the shear layer and have phase lines tilted against the shear to allow downgradient Reynolds stress and energy transfer between the mean flow and the perturbation. After $t_0$ the phase lines of the trapped, growing disturbances become more and more inclined in the direction of the shear, leading to upgradient Reynolds stress, and the perturbation energy decays in the long term. Initially the decaying perturbations are also confined inside the shear layer and have phase lines slightly tilted in the direction of the shear. For these different initial conditions the confinement persists in time if the disturbances have a large horizontal wave number. This often makes the growths or the decays more efficient for short, trapped disturbances than for long disturbances. At small horizontal wave number, these disturbances emit gravity waves which propagate away from the shear layer. Accordingly, below the critical value $k_c = \sqrt{Ri}/d$ the optimal growth decreases rapidly when the horizontal wave number decreases. Nevertheless, the fact that the long disturbances propagate away from the shear layer makes their growth very persistent. For such disturbances, small initial conditions can lead to very spectacular gravity waves going out from the shear layer. It is also noteworthy that in the presence of diffusion the largest optimal growth can occur for wave numbers $k < k_c$. In combination with the persistence, this effect of the diffusion causes the shear layer predominantly to emit outgoing waves, with phase lines tilting upstream and with horizontal wave number smaller than $k_c = \sqrt{Ri}/d$.

It is clear that the analysis of the singular vectors that lead to the largest perturbation-energy growth overstates the ability of the shear layer to spontaneously generate outgoing waves from an initially small perturbation. Indeed, there are only a few singular vectors that lead to significant energy growth. By analysing ensembles of simulations with initial conditions chosen stochastically, but confined in the shear layer, it appears that the perturbation growth is generally much smaller than that predicted by the largest singular vectors. Nevertheless, it appears that the energy persistence found for optimal initial conditions at wave number $k < k_c$ often leads to significant perturbation growth in the long term

when the initial conditions are chosen stochastically inside the shear layer. By contrast, the disturbances with large wave number always die away in the long term.

The fact that decaying and growing waves balance, and that the energy growth in general configuration is not as spectacular as that found for the optimal disturbance, hides an important filtering property of the shear layer. Indeed, the positive shear amplifies disturbances with negative phase-line tilts and damps those with positive phase-line tilts: it completely breaks the symmetry of the initial conditions. Here symmetrical means that over a large ensemble of initial conditions, there are as many waves with positive vertical wave number as there are waves with negative vertical wave number. Comparisons between ensembles of simulations with shear and ensembles of simulations without shear show that, with positive shear, waves with negative momentum fluxes (i.e. propagating downstream) systematically dominate above and below the shear layer. Without shear the initial perturbation confined in a narrow region disperses radiating waves with positive and negative momentum fluxes isotropically. The resulting momentum fluxes are always negative in the case with positive shear, and significantly larger than those found when the initial disturbance disperses in a background fluid at rest. This shows that the impact of the shear on the outgoing momentum fluxes is systematically significant.

It is noteworthy that the problem studied has some points in common with the problem of waves generated by convection. Indeed, it is well established that the shear has an impact on the gravity waves that are generated by convection. With shear, convective waves have phase lines which tilt upstream (in the frame of reference moving with the convection) with height. The mechanisms described in this paper provide the basic explanation of this wave asymmetry. These mechanisms also cause the wave-momentum flux above and below the shear layer to have a sign opposite to that of the shear. The flux is also systematically very large compared with the wave-momentum-flux amplitude measured without shear. Over a rather large ensemble of realizations this amplification always exceeded a factor of 10 when $Ri < 10$. It increases when $Ri$ decreases, and for the simulations presented an approximate relationship was given between the amplification and the stability. This relationship is only qualitative since the flow configuration adopted is highly idealized. Nevertheless, it suggests how amplification factors linking convective forcing and momentum fluxes in shear flows should vary with the flow stability for waves forced by convection.

For more precise applications the approach used in the present paper should be extended to more realistic configurations such as a cold-front jet with a ground surface and a tropopause. These results should also be extended to a stochastically forced shear layer, and to nonlinear configurations.

## Appendix A

### *Discrete direct model*

The matrix $\mathbf{A}$ which represents the discretized evolution equation (9) can be written as:

$$\mathbf{A} = \begin{pmatrix} \underline{\boldsymbol{\Delta}}^{-1} & 0 \\ 0 & \underline{\mathbf{I}} \end{pmatrix} \begin{pmatrix} -\mathrm{i}k\underline{\boldsymbol{U}}\,\underline{\boldsymbol{\Delta}} + \mathrm{i}k\underline{\boldsymbol{U}_{zz}} - \underline{\boldsymbol{a}}\,\underline{\boldsymbol{\Delta}} - \underline{\boldsymbol{a}_z}\,\underline{\partial_z} + \nu\underline{\boldsymbol{\Delta}}^2 & -\mathrm{i}kRi \\ \mathrm{i}k & -\mathrm{i}k\underline{\boldsymbol{U}} - \underline{\boldsymbol{a}} + \nu\underline{\boldsymbol{\Delta}} \end{pmatrix},$$

where the underlined symbols represent the matrices corresponding to the underlined operators. The temporal evolution is then estimated by one forward Euler step followed by successive leap-frog steps. Furthermore, the signal is filtered every time-step by an Asselin

filter with coefficient $\alpha = 0.1$. Starting from the initial conditions $\mathbf{X}_0$ at time $t = 0$, the numerical integration of (9) produces the estimate $\mathbf{X}_p$ at time $t = p\mathrm{d}t$:

$$\mathbf{X}_p = \mathbf{P}\,\mathbf{L}_a{}^{p-1}\,\mathbf{E}_u\,\mathbf{D}\,\mathbf{X}_0 = \mathbf{M}(t)\,\mathbf{X}_0,$$

where $\mathbf{M}(t)$ is the linear model, $\mathbf{D} = \begin{pmatrix} \underline{\mathbf{\Delta}} & 0 \\ 0 & \underline{\mathbf{I}} \end{pmatrix}$ transforms the stream function into vorticity and leaves the buoyancy unchanged in the vector $\mathbf{X}$. The matrix $\mathbf{E}_u$, defined by

$$\mathbf{Y}_1 = \begin{pmatrix} \mathbf{X}_0 \\ \mathbf{X}_1 \end{pmatrix} = \begin{pmatrix} \underline{\mathbf{I}} \\ \underline{\mathbf{I}} + \mathrm{d}t\underline{\mathbf{A}} \end{pmatrix} \mathbf{X}_0 = \mathbf{E}_u\,\mathbf{X}_0,$$

calculates $\mathbf{X}_1$ by one forward Euler step and constructs $\mathbf{Y}_1$ by superposition of $\mathbf{X}_0$ and $\mathbf{X}_1$. In this notation, the matrix $\mathbf{L}_a$, which evaluates the leap-frog step followed by the Asselin filter, can be defined by

$$\mathbf{Y}_p = \begin{pmatrix} \check{\mathbf{X}}_{p-1} \\ \mathbf{X}_p \end{pmatrix} = \begin{pmatrix} \underline{\boldsymbol{\alpha}} & \underline{\mathbf{I}} - \underline{\boldsymbol{\alpha}} + \alpha\mathrm{d}t\underline{\mathbf{A}} \\ \underline{\mathbf{I}} & 2\mathrm{d}t\underline{\mathbf{A}} \end{pmatrix} \begin{pmatrix} \check{\mathbf{X}}_{p-2} \\ \mathbf{X}_{p-1} \end{pmatrix} = \mathbf{L}_a \begin{pmatrix} \check{\mathbf{X}}_{p-2} \\ \mathbf{X}_{p-1} \end{pmatrix},$$

where $\check{\mathbf{X}}_k$ represents $\mathbf{X}_k$ corrected by the Asselin filter. Finally, the matrix

$$\mathbf{P} = (0 \quad \mathbf{D}^{-1})$$

inverts the vorticity towards the stream function and projects back the vector $\mathbf{Y}_p$ onto $\mathbf{X}_p$.

## Appendix B

### *Discrete adjoint model*

The adjoint of the model $\mathbf{M}^*(t)$, relative to the scalar product in (11) can be written as

$$\mathbf{M}^*(t) = \mathbf{D}\mathbf{E}_u{}^*\mathbf{L}_a{}^{*p-1}\mathbf{P}^*\,. \tag{B.1}$$

In (B.1) the fact that the Laplacian operator is self-adjoint is used, so that the operator $\mathbf{D}$ is self-adjoint. The other operators in (B.1) can be written as

$$\mathbf{P}^* = \begin{pmatrix} 0 \\ \mathbf{D}^{-1} \end{pmatrix},$$

$$\mathbf{L}_a{}^* = \begin{pmatrix} \underline{\boldsymbol{\alpha}} & \underline{\mathbf{I}} \\ \underline{\mathbf{I}} - \underline{\boldsymbol{\alpha}} + \alpha\mathrm{d}t\mathbf{A}^* & 2\mathrm{d}t\mathbf{A}^* \end{pmatrix},$$

$$\mathbf{E}_u{}^* = \begin{pmatrix} \underline{\mathbf{I}} & \underline{\mathbf{I}} + \mathrm{d}t\mathbf{A}^* \end{pmatrix},$$

and

$$\mathbf{A}^* = \begin{pmatrix} ik\underline{\underline{\Delta}}\,\underline{U} - ik\underline{U_{zz}} - \underline{\underline{\Delta}}\,\underline{a} - \underline{\partial_z}^*\,\underline{a_z} + \nu\Delta^2 & -ik \\ ikRi & ik\underline{U} - \underline{a} + \nu\Delta \end{pmatrix} \begin{pmatrix} \underline{\underline{\Delta}}^{-1} & 0 \\ 0 & \underline{\underline{I}} \end{pmatrix}.$$

With this notation, the adjoint model first defines the vector

$$\mathbf{Y}_p = \begin{pmatrix} 0 \\ \mathbf{D}^{-1}\mathbf{X}_p \end{pmatrix} = \mathbf{P}^*\mathbf{X}_p,$$

then the operator $\mathbf{L}_a^*$ calculates

$$\mathbf{Y}_{k-1} = \mathbf{L}_a^*\mathbf{Y}_k$$

successively for $k = p + 1, p, \ldots, 2$. The adjoint of the Euler step $\mathbf{E}_u{}^*$ finally calculates

$$\mathbf{X}_0 = \mathbf{X}_1 + \check{\mathbf{X}}_2 + \mathrm{d}t\mathbf{A}^*\mathbf{X}_1.$$

## References


Alexander, M. J., Holton, J. R. and Durran, D. R. 1995 The gravity wave response above deep convection in a squall line simulation. *J. Atmos. Sci.*, **52,** 2212–2226

Blumen, W. 1972 Geostrophic adjustment. *Rev. Geophys. Space Phys.*, **10,** 485–528

Booker, J. R. and Bretherton, F. P. 1967 The critical layer for internal gravity waves in a shear flow. *J. Fluid Mech.*, **25,** 513–529

Boyd, J. P. 1983 The continuous spectrum of linear Couette flow with the beta effect. *J. Atmos. Sci.*, **40,** 2304–2308

Bretherton, C. S. and Smolarkiewitcz, P. K. 1989 Gravity waves, compensating subsidence and detrainment around cumulus clouds. *J. Atmos. Sci.*, **46,** 740–759

Buizza, R., Tribbia, J., Molteni, F. and Palmer, T. 1993 Computation of optimal unstable structures for a numerical weather prediction model. *Tellus*, **45A,** 388–407

Clark, T. L., Hauf, T. and Kuettner, J. P. 1986 Convectively forced internal gravity waves: Results from two-dimensional experiments. *Q. J. R. Meteorol. Soc.*, **112,** 899–925

Drazin, P. G. 1958 The stability of a shear layer in an unbounded heterogeneous inviscid fluid. *J. Fluid Mech.*, **4,** 2201–2214

Farrel, B. F. and Ioannou, P. J. 1993 Transient development of perturbations in stratified shear flow. *J. Atmos. Sci.*, **50,** 2201–2214

Farrell, B. J 1982 The initial growth of disturbances in a baroclinic flow. *J. Atmos. Sci.*, **39,** 1663–1686

Fovell, R., Durran, D. and Holton, J. R. 1992 Numerical simulations of convectively generated stratospheric gravity waves. *J. Atmos. Sci.*, **49,** 1427–1442

Fritts, D. C. 1982 Shear excitation of atmospheric gravity waves. *J. Atmos. Sci.*, **39,** 1936–1952

Holton, J. R. 1983 The influence of gravity wave breaking on the general circulation of the middle atmosphere. *J. Atmos. Sci.*, **40,** 2497–2507

Howard, L. N. 1961 Note on a paper of John W. Miles. *J. Fluid Mech.*, **10,** 509–512

Kershaw, R. 1995 Parametrization of momentum transport by convectively generated gravity waves. *Q. J. R. Meteorol. Soc.*, **121,** 1023–1040

Lacarra, J. F. and Talagrand, O. 1988 Short range evolution of small perturbations in a barotropic model. *Tellus*, **40A,** 81–95

Lott, F. and Teitelbaum, O. 1993 Linear unsteady mountain waves. *Tellus*, **45A,** 201–220

Lott, F., Kelder, H. and Teitelbaum, H. 1992 A transition from Kelvin-Helmholtz instabilities to propagating wave instabilities. *Physics of Fluids A*, **4,** 1990–1997

Miles, J. W. 1961 On the stability of heterogeneous shear flows. *J. Fluid Mech.*, **10,** 496–508

| | | |
|---|---|---|
| Orr, W. M. | 1907 | Stability or instability of the steady motions of a perfect liquid. *Proc. Roy. Irish Acad.*, **A.27,** 9–69 |
| Palmer, T., Shutts, G. and Swinbank, R. | 1986 | Alleviation of systematic westerly bias in general circulation and numerical weather prediction models through an orographic gravity wave drag parametrization. *Q. J. R. Meteorol. Soc.*, **112,** 2056–2066 |
| Queney, P. | 1947 | 'Theory of perturbations in stratified currents with application to airflow over mountains'. Misc. Report No 21. University of Chicago Press |
| Rosenthal, A. J. and Lindzen, R. S. | 1983 | Instabilities in a stratified fluid having one critical level. Part II: Explanation of gravity wave instabilities using the concept of overreflection. *J. Atmos. Sci.*, **40,** 521–529 |
| Rossby, C. G. | 1937 | On the mutual adjustment of pressure and velocity distributions in certain simple current systems. *J. Mar. Res.*, **1,** 15–28 |
| Shepherd, T. G. | 1985 | Time development of small disturbances to plane Couette flow. *J. Atmos. Sci.*, **42,** 1868–1871 |
| Shutts G. J. and Gray, M. E. B. | 1994 | A numerical modelling of the geostrophic adjustment process following deep convection. *Q. J. R. Meteorol. Soc.*, **120,** 1145–1178 |
| Smith, R. | 1979 | The influence of mountains on the atmosphere. *Adv. Geophys.*, **21,** 87–230 |
| Smyth, W. D. and Peltier, W. R. | 1989 | The transition between Kelvin-Helmholtz and Holmboe instability. *J. Atmos. Sci.*, **46,** 3698–3720 |
| Sutherland, B., Caufield, C. and Peltier, W. | 1994 | Internal gravity wave generation and hydrodynamic instability. *J. Atmos. Sci.*, **51,** 3261–3280 |